Soft Matter

PAPER

Cite this: *Soft Matter*, 2018, **14**, 3315

A study of polymer chain diffusion by surface enhanced Raman: effects of plasmonic substrate topology†

Carla D. Mana,[a] Gustavo A. Torchia [b] and J. Pablo Tomba *[a]

Received 2nd January 2018,
Accepted 1st April 2018

DOI: 10.1039/c8sm00017d

rsc.li/soft-matter-journal

We report on a new methodology to track chain interdiffusion between polymer slabs based on Raman enhanced by plasmonic substrates. Diffusion is studied in a deuterated-polystyrene/polystyrene (dPS/PS) polymer pair, designed to provide a well-characterized diffusion behavior. The bilayer, 160 nm thick in total, is supported on a plasmonic substrate that provides local amplification of Raman signals in sample regions of close proximity to it. Gold-based substrates with structures of inverted pyramids, spherical nanoparticles and tipped pillars were investigated. Interdiffusion between dPS and PS is promoted upon annealing and followed *in situ* by dynamic spectral acquisition. A simple model that describes the coupling between the sampled region arising from the plasmonic effect and the diffusion process is employed to interpret spectral evolution data. It is shown that a highly regular topology and surface continuity are key features of the plasmonic substrate in order to provide reliable results. With pyramidal substrates, the most suitable substrates for this application, data are consistent with diffusion coefficients in the range 10^{-13}–10^{-15} cm^2 s^{-1} and dimensions of sampled regions below 40 nm. The strategy provides a reliable labeling-free technique to investigate polymer interdiffusion on the nanoscale.

1. Introduction

Polymer interdiffusion and chain dynamics have been topics of longstanding interest in polymer science due to their important role in applications that involve welding, adhesion, coating or blending. The topic also has an impact on new applications based on polymer nanocomposites, where changes in chain dynamics by the presence of nano-sized objects (tubes, particles, sheets, wires) influence the processing, permeability and mechanical, electrical, optical or magnetic properties of those materials.[1–3]

Several experimental techniques have been employed in the past to investigate polymer interdiffusion, with their own strengths and drawbacks. Ideally, a technique to study polymer diffusion should provide spatial resolution to resolve chain transport in the range of a few to hundreds of nanometers, as characteristic diffusion distances of very high molecular weight species lie in this range. Another important feature is the ability to track diffusion without resorting to chemical labeling to improve contrast. Chemical labeling not only complicates sample preparation but also changes the thermodynamic interactions of the system, which in turn influences the chain dynamics.

It is hard to find techniques that meet all these requirements. Many of the diffusion data published in the literature have been acquired using powerful high-resolution techniques such as Forward Recoil Spectrometry (FRES) or Nuclear Reaction Analysis (NRA), able to resolve motions from large sequences of polymer segments to the entire polymer chains.[4,5] Neutron Reflectometry (NR) has also been extensively employed to probe polymer interfaces on a scale of a few nanometers.[6] Fluorescence Energy Transfer (FRET) has been a major tool to investigate polymer diffusion during latex film formation, on a spatial scale of tens of nm.[7] However, all the above-mentioned techniques require isotopic (FRET, NRA, NR) or fluorescence (FRET) labeling to track chain diffusion.

Microspectroscopies, particularly Raman, have also been employed to investigate polymer interdiffusion.[8,9] As an advantage, the technique does not need sample preparation to resolve chain diffusion as it uses the natural spectroscopic contrast arising from the particular chain structure of each compound. The technique can be used in several exploration modes such as lateral or depth profiling. As a disadvantage, Raman microscopy is penalized with a relatively poor diffraction-limited spatial resolution, on the order of visible (laser)

[a] *Institute of Materials Science and Technology (INTEMA), National Research Council (CONICET), University of Mar del Plata, Mar del Plata, Argentina. E-mail: jptomba@fi.mdp.edu.ar*

[b] *Centro de Investigaciones Opticas-CONICET-CICBA-UNLP, La Plata, Argentina*

† Electronic supplementary information (ESI) available. See DOI: 10.1039/c8sm00017d

wavelength. The above fact limits its application to the study of diffusion of oligomeric components, on a much coarse micron scale.[10] Dynamic light scattering has also been used in the past to study polymer interdiffusion, sharing with microspectroscopies the advantage of not requiring chemical labeling and the range of diffusion coefficients that can be effectively tracked, above 10^{-10} cm^2 s^{-1}.[11,12]

Recently, we have started to explore a strategy based on Surface Enhanced Raman Spectroscopy (SERS) to investigate the phenomenon of polymer diffusion on a finer (nanometer) scale, taking advantage from the exceptional amplification of Raman signals provided by the technique in sub-diffractional sized environments.[13] It is based on the dramatic enhancement of cross-sections of molecules that occurs in the presence of plasmons of noble metals, delivered by suitably designed substrates. Signal amplification by surface plasmons has also been exploited in diffusion studies of polymeric particles by dynamic light scattering.[14] In SERS experiments, the geometry of the metallic substrate plays a major role in the experimental setup. For instance, the local amplification that gives rise to the SERS effect occurs in a confined region of space, the so-called substrate hotspot, whose dimensions are strongly coupled to the topological characteristics of the metal substrate. One of the main points in our strategy is the tuning of the size of this hotspot to the characteristic distances for polymer diffusion to be detected. Spectral reproducibility is also directly tied to substrate topological regularity. Substrate geometry also determines the spatial framework on which chain transport is produced, and so, the diffusion models necessary for data interpretation.

In this work, we report on diffusion experiments on a series of SERS substrates with different geometry. The diffusion pair under study is a deuterated polystyrene–polystyrene (dPS–PS) polymer pair, designed to provide a well-characterized diffusion behavior. Gold-based, commercially available, SERS substrates with structures of inverted pyramids, spherical nanoparticles and tipped pillars are investigated. A simple model to describe the coupling between plasmonic effects and chain diffusion is introduced. Interdiffusion between dPS and PS is promoted upon annealing and followed *in situ* by dynamic spectral acquisition. Changes in characteristic Raman bands of dPS and PS species over time are interpreted in terms of the above-mentioned model, which provides a framework to understand the influence of substrate geometry on the diffusion process as well as the order of diffusivities and spatial scale that can be effectively tracked by the experiment.

2. Experimental

Three commercial SERS substrates were used: Klarite 313 (Renishaw Diagnostics), QSERS (Nanova Inc.) and SERS Silmeco (Silmeco). All substrates were provided as a chip made on a silicon wafer with a SERS active area of about 4 × 4 mm^2 and they were used as received. Images of the SERS substrates were obtained with a Scanning Electron Microscope (SEM) JEOL JSM-460LV using accelerating voltages between 10 and 25 kV and magnifications between 3000 and 30 000.

The polymers for diffusion experiments, deuterated polystyrene (dPS) and polystyrene (PS), were purchased from Polymer Source. The samples are nearly monodisperse ($M_w/M_n < 1.1$), with molecular weights of 236 500 g mol^{-1} (dPS) and 215 000 g mol^{-1} (PS). Glass transition temperatures (T_g) of the polymers are similar and about 100 °C. Thin polymer films were prepared by spin-coating from dilute solutions in toluene. The thickness of the films was controlled by adjusting the concentration of the solution used, the angular velocity and the time steps, based on a previous protocol developed in the group. The films used were of (80 ± 5) nm and were measured on glass substrates with a KLA Tencor 100 profilometer.

Polymer bilayers for diffusion experiments were prepared as follows. First, dPS was deposited onto the SERS subtrate by spin coating. Separately, a free standing PS film was deposited by the same technique but onto a water-soluble potassium bromide (KBr) substrate. KBr was then removed with water to obtain a free standing PS film, which was subsequently deposited onto that of dPS. Bilayer films were left in a vacuum at 40 °C for 1 day to remove solvent traces. The configuration of the films and substrates for diffusion experiments is schematically shown in Fig. 1.

SERS and Raman spectra were taken with a Renishaw inVia Reflex Raman microscope equipped with a charge-coupled device (CCD) detector (1040 × 256 pixels). Spectra were primarily collected using a 785 nm laser in combination with a grating of 1200 lines per mm; a 514 nm laser was also tested. Instrumental filters were used to reduce the laser power at 10% in order to keep actual values of incident power below 7.5 mW. Diffusion between PS and dPS was promoted by subjecting the composite films to temperatures above T_g in a Linkam THMS 600 hot stage, under a nitrogen atmosphere, see Fig. 1. Raman spectra were taken *in situ* with a Renishaw inVia Reflex using a long-distance objective Leica 50× (NA: 0.55). The sampled area was adjusted by using 6 pixels of the CCD in combination with 65 μm of slit aperture (regular confocality). Under these conditions, the sampled area corresponds to a region of about 15 μm diameter.

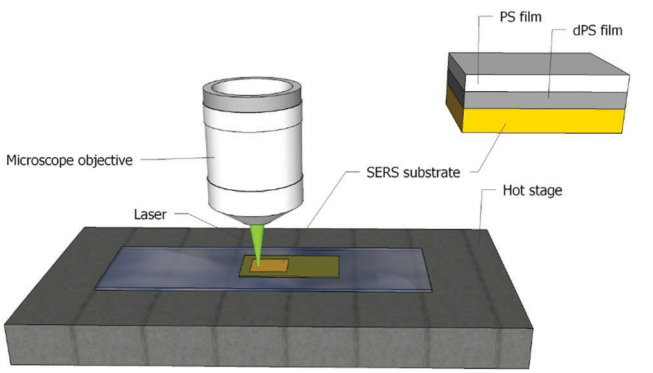

Fig. 1 Scheme of the experimental setup. The dimensions of the active area of the SERS substrate is about 4 × 4 mm^2. The area of the substrate illuminated by the laser beam is about 15 μm in diameter.

Acquisition time for each spectrum was 2 seconds with 5 accumulations. Spectra were taken at 5 different spots on the sample and the results averaged. A calibration curve was built to relate the weight fraction of each of the polymers with their individual contributions to the Raman spectrum, see Fig. S1, ESI.† Homogeneous polymer blends containing different proportions of PS and dPS were prepared from dissolution in a common solvent (benzene) followed by freeze drying. Raman spectra of the blends were processed using the linear decomposition method to obtain the plot shown in Fig. S1 (ESI†); see more details elsewhere.[15]

Computer simulations of the diffusion problem in the transient regime for a bimensional geometry were carried out using Abaqus software and a Finite Element Method based algorithm; see more details in the ESI.† Transport was assumed to be Fickean and characterized by a constant diffusion coefficient.

3. Results and discussion

Characterization of experimental setup components

Conventional Raman spectra of the pure polymers are shown in Fig. 2 for the fingerprint region. The strong band at 1000 cm^{-1} in PS can be ascribed to aromatic in plane C–H deformation vibrations, whereas the band at 960 cm^{-1} in the fully deuterated PS (dPS) is assigned to the same vibrational mode.[16] The difference in the spectral profiles generates the contrast between components necessary to individually resolve chain diffusion by Raman spectroscopy.

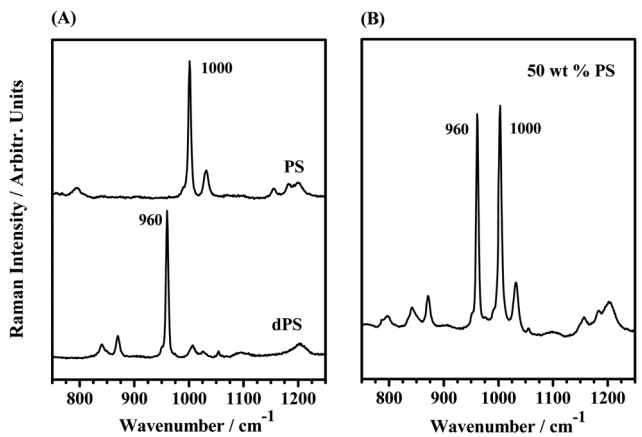

Fig. 2 Raman spectra of (A) individual components; (B) physical blend between them.

Fig. 2(B) shows the Raman spectrum of a physical blend between PS and dPS, prepared by casting from a common solvent. The spectrum shows features of both components, with prominent bands at 960 and 1000 cm^{-1}. The composite blend spectrum is simply the addition of those of the pure components without significant shifting and/or broadening of Raman peaks due to interactions. The fact that the intensities of peaks at 1000 and 960 cm^{-1} are comparable for the 50 wt% blend indicates that Raman cross sections of dPS and PS components are also similar. This and other blends were used for calibration purposes to relate the band intensity with local composition; see Experimental part and subsequent sections.

Fig. 3 shows SEM images of the substrates tested. Klarite, shown in Fig. 3(A), presents a periodic square-based inverted pyramidal geometry. Lateral dimensions of the pyramids are about 1.5 μm, whereas the heights is about 1 μm according to the manufacturer. The topology of QSERS, Fig. 3(B), is particle-based. The lighter areas correspond to particle aggregates with diameters of about 60 nm, according to the image. These particles are supported by a base made of smaller particles, the darker areas of the image, with diameters of about 15 nm according to the manufacturer. Fig. 3(C) shows images of a SILMECO substrate, which is based on silicon-based silver-tipped pillars. The pillars have an overall length of about 600 nm, whereas the silver tip diameter is about 150 nm. One of the problems that one may anticipate with this substrate is that it would be difficult to deposit a continuous layer of polymer due to the significant space between pillars.

Thin polymer films were deposited onto each of these substrates and Raman spectra measured. Very good data quality was observed in all the cases, except for pillar-based substrates (see Fig. S2, ESI†). Fig. 4(A) shows Raman spectra of polymeric films 80 nm thick deposited onto pyramidal and spherical-type structures, acquired under similar instrumental conditions. Both responses are comparable, but somewhat higher in the pyramidal substrate. In earlier work, we have shown that the response of dPS films of the same thickness but on glass did not show Raman peaks, indicating that conventional Raman scattering cannot be detected for that level of film thickness.[13] Therefore, the responses shown in Fig. 4(A) can be entirely ascribed to the SERS effect. Notice that the region illuminated by the laser beam is about 15 μm in diameter so

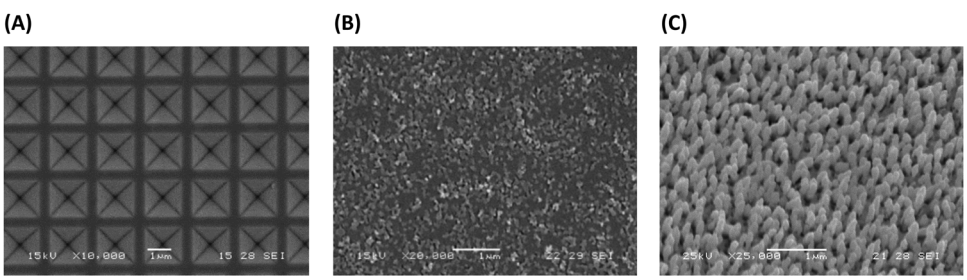

Fig. 3 SEM images of the SERS substrates tested.

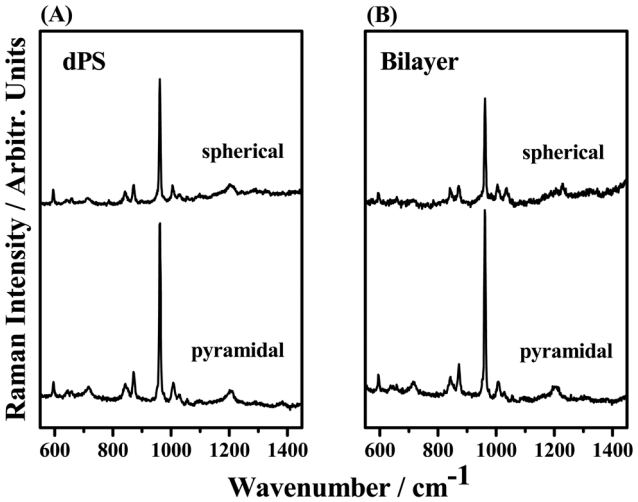

Fig. 4 (A) SERS spectra of 80 nm thin films of dPS over pyramidal- and spherical-type substrates. (B) SERS spectra of polymer bilayers, with dPS at the bottom in contact with the SERS substrate, and PS on top. Both PS and dPS films were 80 nm thick.

the SERS signal most likely originates from several hotspots. The lack of performance of the pillar-based platform for this specific application can be explained in terms of their reported mechanism of action, which involves leaning of group of pillars to create hotspots between silver tips.[17] Film deposition by spin coating may not be the best method to promote that effect; see Fig. S2, ESI.†

Fig. 4(B) shows Raman responses of film bilayers, composed of a dPS film (80 nm thick) at the bottom, in direct contact with the SERS substrate, and a second PS film (80 nm thick) on top of it. SEM images of bilayers are shown in Fig. S3, ESI.† We observe that the spectral features correspond entirely to dPS, without signatures of the PS film. The lack of signal of PS further confirms that: (i) conventional Raman scattering is not significant and the observed response is entirely due to the SERS effect; (ii) the dimensions of the substrate hotspot are below the thickness of the dPS layer, otherwise, the signal from the PS film should also have been observed. The consequences of these observations in the context of a mathematical model for the process will be discussed in the next section.

Modeling of the SERS-based diffusion experiment

In this section, the mathematical framework needed to interpret and quantify polymer diffusion from SERS experiments is presented. Fig. 5 shows a series of geometries that exemplify the elements of the SERS setup, that is, the polymer films (grey), the substrate (gold) and its hotspot (red region). Dimensions and shape of the hotspot are approximated but based on simulations of the plasmonic effects reported in the literature.[18,19] Fig. 5(A) shows a one-dimensional scheme, whereas Fig. 5(B) and (C) represent two-dimensional geometries ascribable to pyramidal and particle-based substrates.

The Raman response of the systems shown in Fig. 5 is a result of two contributions: (i) Raman scattering of the polymer chains located in the hotspot, whose response is dramatically enhanced by their proximity to the metal substrate; (ii) conventional Raman scattering of polymer chains with low cross-section, located out of the hotspot. Despite the number of these chains being certainly much larger than those contained in the hotspot, their scattering is not significant because the polymeric films in our experimental setup are actually very thin, as discussed in Fig. 4. Therefore, as long as the polymeric films are thin enough, the spectral features observed in the data reported in Fig. 4 or 5 can be interpreted as entirely arising from the polymer chains located in the substrate hotspot. Under this assumption, the information captured by each Raman spectrum is described as a cumulative response over all the chemical species within the substrate hotspot or detection zone. Mathematically, the concept is represented by a convolution integral:

$$\mathrm{cwf}(t) = \frac{\int_{\Omega} I(\mathbf{x})\varphi(\mathbf{x},t)\mathrm{d}\mathbf{x}}{\int_{\Omega} I(\mathbf{x})\mathrm{d}\mathbf{x}} \quad (1)$$

where $\mathbf{x}$ represents the spatial x, y, z coordinates, $\varphi(\mathbf{x},t)$ the concentration field of the chemical species, $I(\mathbf{x})$ the distribution function of intensity reinforcement of the substrate and Ω the dimensions of the hotspot. Time-variations in the concentration field due to the diffusion will be seen as changes in cwf, so, the monitoring of cwf is expected to reveal chain diffusion dynamics. At the annealing time t, the SERS response of a given chemical species is a product of its weight fraction and the substrate- and distance-to-substrate-dependent SERS response I, integrated over the hotspot. When this calculation is repeated for each diffusion time, it yields a profile of cumulative weight fraction.

To calculate cwf profiles, models for polymer diffusion and the SERS response are needed. Note that the geometry of the

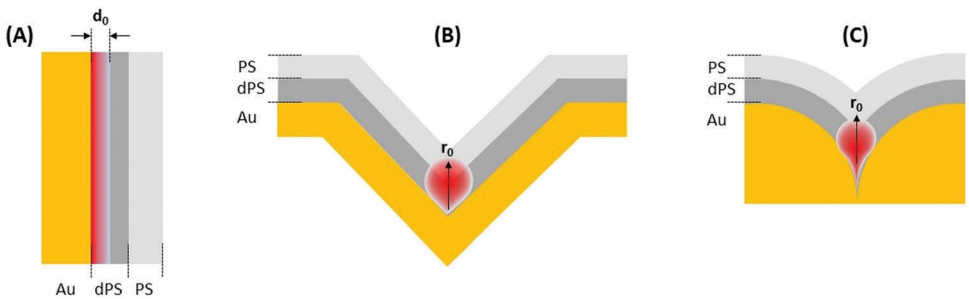

Fig. 5 (A) One-dimensional description of the diffusion experiment; bi-dimensional representation of pyramidal (B) and spherical (C) geometries. Hotspot dimensions are characterized by d_0 (one-dimensional case) and by r_0 in the case of pyramidal and spherical substrates.

substrate impacts the choice of both models and that the integral given by eqn (1) may need to be performed in one, two or three dimensions. From the point of view of the diffusion problem, it is thought that the bi-layered polymer film geometry copies the surface topology of the substrate, thus creating regions with diffusion gradients of different dimensionalities. For instance, in the case of pyramidal structures, see Fig. 5(B), at the pyramidal walls or at the flat areas connecting the pyramids, diffusion ought to be mostly one-dimensional, as compositional gradients between polymer films are essentially normal to the substrate surface and rather uniform at these regions. However, at regions located near the pyramidal tip, compositional gradients are multidimensional, due to the shape of the tip. A similar situation is anticipated in spherical-type substrates, see Fig. 5(C), where, depending on the particle radius and the ability of the polymer film to copy the substrate topology, diffusion may be either one dimensional on top of the spheres or more likely multidimensional in interparticle gaps.

The second component of the calculations is the description of the plasmonic effect, which finally determines the localization of electrical field reinforcements $I(\mathbf{x})$ and overall dimensions of the hotspot Ω. When the electromagnetic wave (*i.e.* visible laser) interacts with a metal substrate, the wave may excite localized surface plasmons on the surface, resulting in amplification of the electromagnetic electric field. Consequently, a large enhancement of Raman scattering intensity arises. This light concentration is highly localized and it occurs preferentially in sharp features of the plasmonic material. It depends on the metal, on substrate geometry and on the refractive index of the surrounding medium. The effect can be modelled by solving the Maxwell formalism describing the electromagnetic phenomenon for the specific substrate geometry.[20] For instance, Vernon *et al.* and Li *et al.* have carried out simulations of electric field distributions by the finite-difference time-domain method for the case of pyramidal-structured substrates and they have shown that the region of maximum field reinforcement is mostly located at the pyramidal pits, as seen in Fig. 5(B).[18,19] In the case of spherical-structured substrates, major enhancements of electric fields are predicted at specific points on the surface of the sphere for the case of an isolated sphere.[21] The effect is highly dependent on the particle diameter. For systems comprising several particles, major enhancements arising from coupled plasmon resonance are found at the particle joints, as seen in Fig. 5(C), whose magnitude is highly dependent on the gap between particles.[21] Therefore, the enhancement effect in Raman signals is not expected to be uniform in the spherical substrate due to the non-uniform distribution of particle diameters and/or interparticle gaps.

Cumulative weight fraction profiles were calculated for the 1-D and 2-D models of the system represented by Fig. 5(A) and (B). In all the cases, the thickness of each of the polymer layers was set to 80 nm, with dPS in direct contact with the substrate and PS on top. Diffusion was assumed to be described by a Fickean constant diffusion coefficient D. No-flux boundary conditions were imposed; see ESI† for more details on numerical resolution. The substrate hotspot is described as a characteristic finite-size region, measured from the substrate surface, where the Raman signal is amplified. We assume that beyond that region, the substrate does not yield a Raman response. In the one-dimensional case, this characteristics distance is defined as d_0 (see Fig. 5(A)) whereas in the bi-dimensional case it is defined as r_0, a radius measured from the pyramidal tip (see Fig. 5(B)).

Fig. 6 shows PS cwf profiles generated with different values of D and fixed values of d_0 or r_0 (40 nm). D values were varied in the range 10^{-13}–10^{-14} cm^2 s^{-1}, whereas the time scale covered was about 30 min. For instance, at 10 min, characteristic diffusion distances calculated as $2(Dt)^{0.5}$ are in the range between 50 and 150 nm. Overall, the PS cwf profiles show a typical diffusive behavior, with an increase with time that reflects the transport of PS chains from the top film to the hotspot, located adjacently to the metallic substrate, and the consequent motion of dPS chains out of it. It occurs at different rates, depending on the values of D. The increase of cwf slows down as the system approaches equilibrium. As PS and dPS films have the same thickness, PS cwf at equilibrium should be 0.5. Comparing predictions of 1-D and 2-D models we found differences. The evolution towards the equilibrium state in the 2-D case is smooth and not as steep as in the 1-D case. Overall, 2 and 3-D geometries tend to smooth cumulative diffusive responses in comparison with the 1-D case and the results of the simulations confirm that fact.[22] The time required to reach

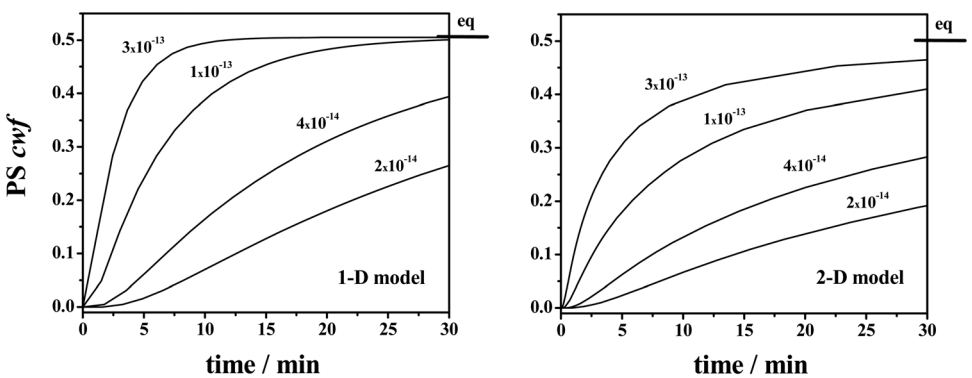

Fig. 6 Simulated PS cwf profiles for a range of D/[cm^2 s^{-1}] values. d_0 (1-D) or r_0 (2-D) were set to 40 nm.

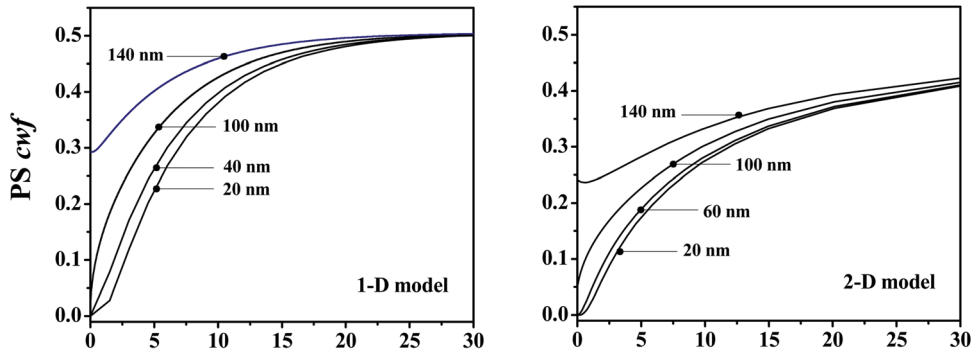

Fig. 7 Effect of the dimensions of the hotspot on the simulated PS cwf profiles, for a value of $D = 10^{-13}$ cm^2 s^{-1}.

equilibrium is also very different. Whereas for D values above 1×10^{-13} cm^2 s^{-1} the equilibrium state is reached in the time-scale of the experiment for the 1-D example, the system is in all the cases far from equilibrium in the 2-D case.

Fig. 7 shows the influence of the dimension of the hotspot on PS cwf profiles. Simulations were carried out with a single value of $D = 10^{-13}$ cm^2 s^{-1} and a range of values of d_0 or r_0 (20–140 nm). These simulations are important to understand the influence of this somewhat uncertain parameter on the cwf profiles. It is seen that the predicted profiles are not very different for hotspot dimensions well below the position of the original interface (80 nm). Major differences are found when d_0 or r_0 are above that value. Numerical simulations suggest that either for pyramidal or spherical substrates, r_0 is rather below 40 nm.[18,21] The experiments on film bilayers shown by Fig. 4 confirm that the value is at least below the thickness of the dPS layer (80 nm), otherwise, signal from the PS layer should have been detected. On that basis, we will assume that reasonable values for r_0 and d_0 are 40 nm, which can be well taken as an indication of the spatial resolution of the methodology.

Comparison with experimental data

Polymer diffusion between dPS and PS was promoted by annealing the composite specimens at several temperatures above T_g of the polymers. Periodically, Raman spectra were acquired to track spectral changes upon annealing. Let's first discuss what would be the expected ranges of variation of spectral features for this diffusion pair. As in all the cases shown, the dPS film was in direct contact with the SERS substrate whereas that of PS was placed on top; the case of no mixing should only reveal spectral features of dPS, as shown in Fig. 4(B). On the other hand, for the molecular weights employed in this work (200 000 g mol^{-1}) a polymer blend between dPS and PS is predicted to be in a single phase (homogeneous) region at the temperatures of the experiment.[23] Therefore, the state of equilibrium corresponds to that of full mixing. As the thicknesses of each of the layers are identical, that state should correspond to a mixture with about 50 wt% in each of the components, and a spectrum similar to that shown in Fig. 2(B), with peaks at 960 cm^{-1} (dPS) and 1000 cm^{-1} (PS) of similar intensity.

Fig. 8 shows the spectral evolution observed in both pyramidal and spherical-based SERS substrates, at several temperatures. Notice that in all the cases, the SERS spectra at zero time primarily show spectral features of the dPS component. With increasing time, the characteristic features of the PS component appear. Data obtained with the pyramidal substrate show a smooth increase of the band at 1000 cm^{-1}, faster at 175 than at 160 °C. At 175 °C, and after 40 min of annealing, the system approaches the equilibrium state, as seen by the similar intensities of peaks at 970 and 1000 cm^{-1}. The data show that at 160 °C the system is still far from equilibrium, even after 333 min of annealing. In all the cases, we found excellent repeatability and reproducibility even at high temperature; for a more detailed analysis see elsewhere.[13]

Data obtained with sphere-based substrates show similar features to those above-discussed. Initially, the spectra are very close to those of pure dPS. After several minutes of annealing, the PS contribution emerges in the spectral profile, as reflected by the Raman band at 1000 cm^{-1}. At 175 °C, the rate of appearance of that band is comparable to that found in the pyramidal-based ones. At 185 °C the rate of appearance is faster than that at 175 °C, but data fluctuations are observed; see for instance the spectra at 30, 81 and 90 min. This is rather common in spherical-based and different from pyramidal substrates, which always showed a steady increase of PS intensity. Overall, the reproducibility delivered by spherical-substrates was not as good as that found in their pyramidal-based counterparts.

The results shown in Fig. 8 can be converted to cwf profiles by translating the information of each Raman spectrum to weight fractions *via* a calibration curve (see Experimental section and ESI†). Fig. 9 shows experimental PS cwf values obtained in this way. Overall, the experimental data behave as illustrated in computer simulations: PS cwf profiles show an initial rapid increase and a slow down as the system approaches equilibrium, in a window of diffusion times not longer than about 200 min. The data generated with the pyramidal substrate is much smoother, whereas those obtained with the spherical geometry have much more scatter, although the overall data features are similar. An increase in annealing temperature increases the rate of growth of PS cwf, which is consistent with a temperature activated diffusion process conducted at temperatures well above that critical for phase separation.

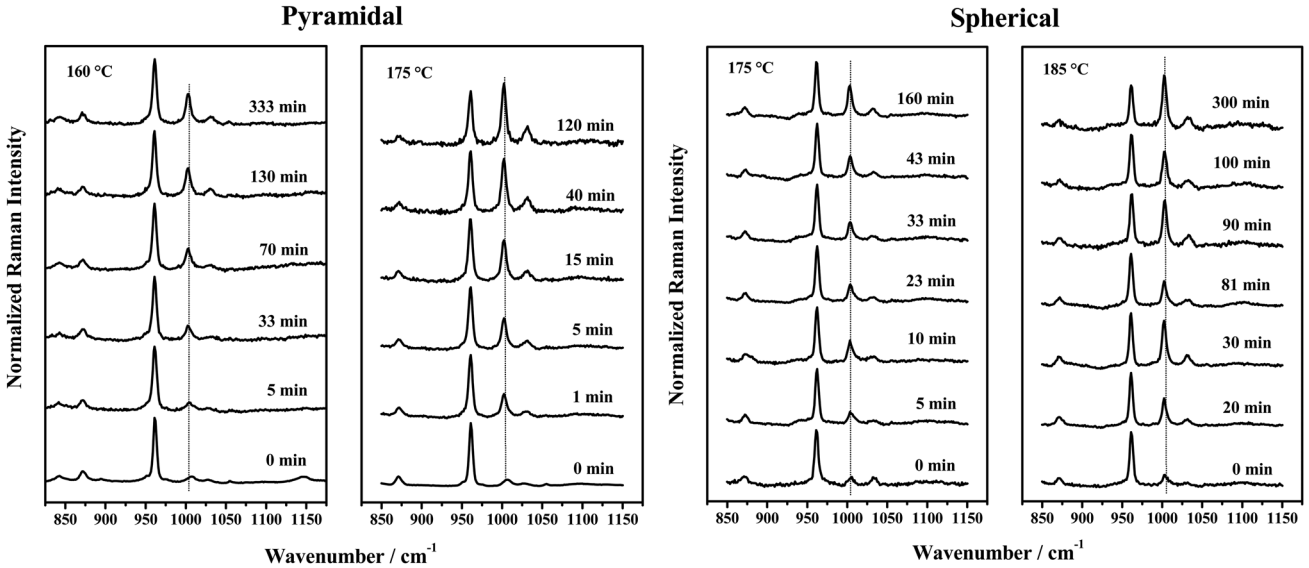

Fig. 8 Spectral evolution upon annealing for pyramidal- and spherical substrates.

A test for data consistency is the comparison of PS cwf profiles with model predictions, which implies the description of both diffusive and plasmonic effects. On the diffusion side, the behavior of the PS–dPS polymer pair can be analyzed in terms of ''fast'' and ''slow'' polymer interdiffusion theories.[24,25] Both theories predict interdiffusion coefficients as the product of a thermodynamic factor, dependent on the Flory–Huggins interaction parameter, and a kinetic one, expressed as a combination of monomeric mobilities, typically embodied in the form of tracer diffusion coefficients.[26] Tracer diffusion coefficients measure the diffusion of a dilute concentration of polymer chains on a matrix of the other polymer; when polymers are the same and with identical molecular weights, the case is called self-diffusion. In the case of interdiffusion, if polymers are chemically similar and with identical molecular weights, the kinetic factor is dominated by a single self-diffusion coefficient, without composition dependency. Besides, if thermodynamic interaction is neglected, both fast and slow theories predict that interdiffusion coefficients will be equal to that of self-diffusion. The interdiffusion between PS and dPS is one of these cases. As glass transition temperatures are similar and the thermodynamic interaction is very weak, no effects of composition on the interdifussion coefficients are expected and a single composition-independent interdiffusion coefficient ascribable to that of self-diffusion can be used to describe the problem. Tracer and self-diffusion coefficients for this polymer pair are available in the literature.[27] For instance, at 170 °C, $D = 1.1 \times 10^{-13}$ cm^2 s^{-1} is found. Using the Williams–Landel–Ferry equation (WLF) for PS, diffusion coefficients at other temperatures can be predicted; see ESI.† The WLF equation yields D values of 4.7×10^{-15} cm^2 s^{-1} (150 °C), 1.9×10^{-14} cm^2 s^{-1} (160 °C) and 2.8×10^{-13} cm^2 s^{-1} (185 °C). On the plasmonic side, it has been discussed that values of about 40 nm represent reasonably well the dimensions of the hotspot, therefore d_0 and r_0 were fixed at 40 nm for 1-D and 2-D simulations, respectively. Modelling is completed assuming that the thickness of each of the slabs is 80 nm. Dotted lines in Fig. 9 correspond to model simulations for 1-D whereas continuous lines represent the 2-D case.

For pyramidal substrates, the 1-D model predicts a rapid growth of PS cwf and an equilibrium state achieved in about 100 min at 160 °C and less than 10 min at 185 °C. None of the data obtained on pyramidal substrates follow that behavior, and in all the cases equilibrium is achieved at much longer times than those predicted. However, experiments follow remarkably well 2-D model predictions, at all the temperatures. This confirms the results of plasmonic simulation with regard to the localization of the hotspot. If the hotspot were located at the pyramidal walls or at the flat areas connecting the pyramids, the diffusion captured ought to be mostly one-dimensional, as compositional gradients between polymer films are essentially normal to the substrate surface and rather uniform at these regions. This is definitively not the case here. The hotspot appears to be located near the pyramidal tip and it senses mass transport driven by multidimensional compositional gradients due to the shape of the tip.

The results obtained from spherical substrates are less reliable than those found with pyramids, besides the evident oscillations and bumps observed in the experimental data. The data appear closer to the 1-D predictions at 160 °C, but depart from that model at 175 °C or 185 °C. There may be several reasons for this behavior. On one hand, we believe that at low annealing temperature, the polymer film placed on the top (PS) remains essentially flat, making contact with that placed at the bottom only at the top of the particles, which would explain the 1-D behavior. At higher temperature, bending of the top film to promote more intimate contact with that on the bottom is likely to occur, which would explain the closer adherence to a 2-D behavior. The duplicity in particle diameter may well explain the bumps and lack of regularity observed in the experiment.

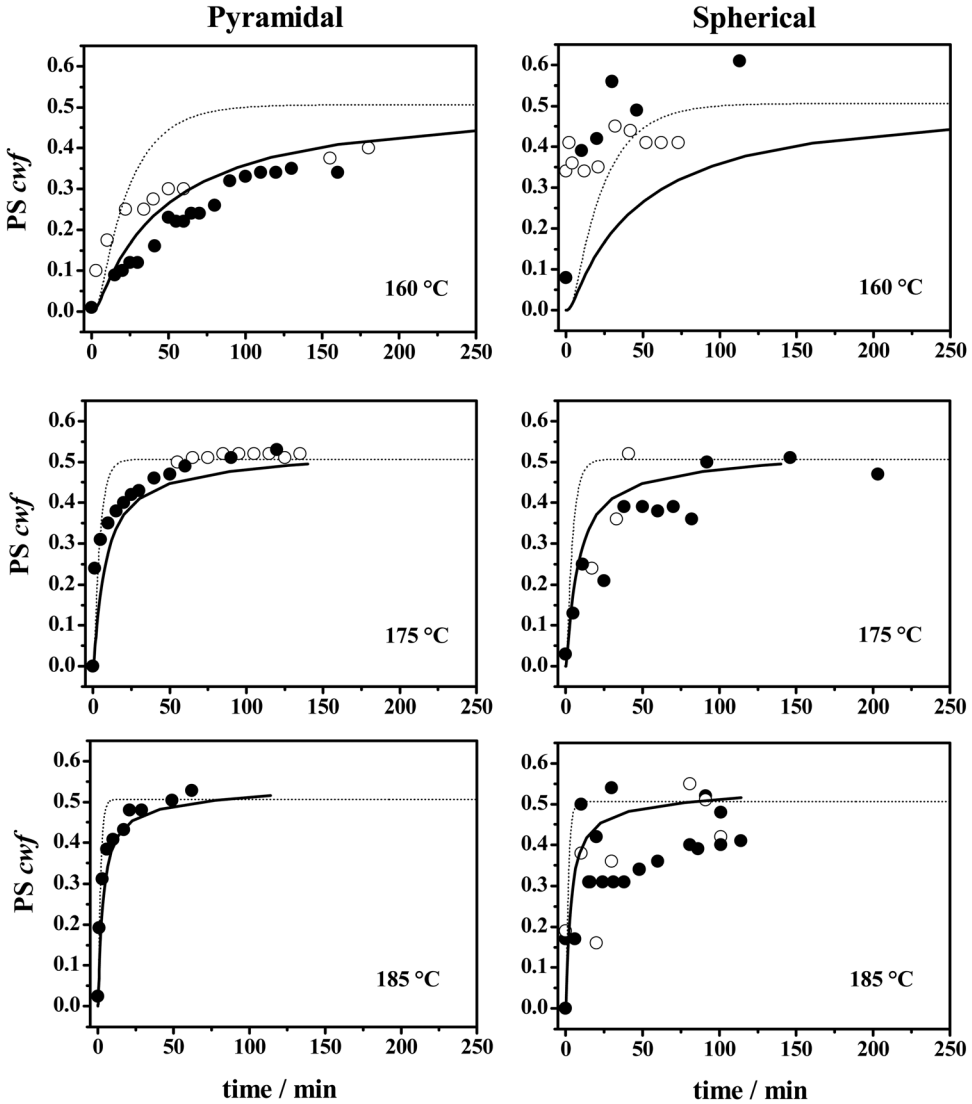

Fig. 9 Profiles of cumulative weight fraction at several annealing temperatures for the two types of substrates. Open and filled symbols represent data of independent experiments. Lines represent calculations with 1-D (dotted) and 2-D (solid) models.

Multiple diameters with non-uniform interparticle gaps generate hotspots with different dimensions and characteristics, which respond differently in terms of Raman signal amplification, thus generating a convoluted response much more difficult to interpret.

4. Conclusions

It has been shown that plasmon-enhanced Raman experiments provide a reliable tool to measure polymer interdiffusion at a level of spatial resolution without precedence for conventional Raman microscopy. As anticipated, the topology of the SERS substrate plays a major role in the experiment. A compromise between: (i) surface continuity, to properly hold the polymer films; (ii) surface irregularity, necessary to promote the Raman enhancement effect; (iii) periodicity, to produce this enhancement in a uniform and reproducible fashion; has shown to be difficult to meet. Substrates based on elongated structures, such as pillars, failed at supporting the polymer films, despite their superb ability to detect traces of components in other applications. Spherical substrates with non-uniform particle distribution generates data that reveal either non-uniform contact between polymer films or non-uniform Raman enhancement effects. The best results for this application were found in substrates with a structure of periodic inverted pyramids, where reliable data were obtained under most of the conditions. Interdiffusion coefficients in the range 10^{-13}–10^{-15} cm^2 s^{-1}, characteristic of high-molecular weight polymers, were effectively tracked.

The use of a simple 2-D model that combines bi-dimensional mass transport between films and the plasmonic phenomena captures very well the essence of the experiment and shows very good agreement with the experimental data. The lack of agreement with the 1-D model strongly supports the fact that the

substrate hotspot is located at the pyramidal tips, as predicted by plasmonic simulations. The use of substrates with highly regular topology guarantees a reliable distribution of hotspots but also facilitates rigorous modeling of both diffusion and plasmonic effects. A full 3-D model of the process is currently underway with the aim of directly characterizing diffusion coefficients by data fitting. Overall, surface-enhanced Raman appears as a promising, label-free technique, suitable for diffusion studies of high molecular weight species, with prospective applications in studies of chain dynamics in the presence of nano-sized objects.

Conflicts of interest

There are no conflicts to declare.

Acknowledgements

This research was possible thanks to the support of ANPCYT (PICT14-1919) and to scholarships provided by ANPCYT and by CONICET.

References

1 J. Choi, M. J. A. Hore, J. S. Meth, N. Clarke, K. I. Winey and R. J. Composto, *ACS Macro Lett.*, 2013, **2**, 485–490.
2 S. Gam, J. S. Meth, S. G. Zane, C. Chi, B. A. Wood, K. I. Winey, N. Clarke and R. J. Composto, *Soft Matter*, 2012, **8**, 6512–6520.
3 J. Choi, N. Clarke, K. I. Winey, R. J. Composto and B. Akgun, *ACS Macro Lett.*, 2014, **3**, 886–891.
4 R. J. Composto, E. J. Kramer and D. M. White, *Macromolecules*, 1988, **21**, 2580–2588.
5 U. K. Chaturvedi, U. Steiner, O. Zak, G. Krausch, G. Schatz and J. Klein, *Appl. Phys. Lett.*, 1990, **56**, 1228–1230.
6 S. Copp, S. Gabriele, A. M. Jonas, J. Jestinc and P. Damman, *Soft Matter*, 2011, **7**, 9951–9955.
7 J. K. Oh, J. P. Tomba, X. Ye, R. Eley, J. Rademacher, R. Farwaha and M. A. Winnik, *Macromolecules*, 2003, **36**, 5804–5814.
8 J. P. Tomba, J. M. Carella and J. M. Pastor, *Macromolecules*, 2009, **42**, 3565–3572.
9 A. C. De Luca, G. Rusciano, G. Pesce, S. Caserta, S. Guido and A. Sasso, *Macromolecules*, 2008, **41**, 5512–5514.
10 J. P. Tomba, *Soft Matter*, 2016, **12**, 4510–4513.
11 U. Murschall, E. W. Fischer and Ch. Herkt-Maetzky, *J. Polym. Sci., Polym. Lett. Ed.*, 1986, **24**, 191–197.
12 M. G. Brereton, E. W. Fischer, G. Fytas and U. Murschall, *J. Chem. Phys.*, 1987, **86**, 5174–5181.
13 C. D. Mana and J. P. Tomba, *J. Raman Spectrosc.*, 2017, **48**, 425–431.
14 M. A. Plum, W. Steffen, G. Fytas, W. Knoll and B. Menges, *Opt. Express*, 2009, **17**, 10364–10371.
15 J. P. Tomba, E. de la Puente and J. M. Pastor, *J. Polym. Sci., Part B: Polym. Phys.*, 2000, **38**, 1013–1023.
16 G. Socrates, *Infrared and Raman Characteristic Group Frequencies*, J. Wiley and Sons, West Sussex, England, 3rd edn, 2006.
17 M. S. Schmidt, J. Hubner and A. Boisen, *Adv. Mater.*, 2012, **24**, OP11–OP18.
18 K. C. Vernon, T. J. Davis, F. H. Scholes, D. E. Gómez and D. Lau, *J. Raman Spectrosc.*, 2010, **41**, 1106–1111.
19 J. Li, X. Xu, Y. Wang, M. Wang, Z. Dong, W. Tian, J. Sun, C. Zhang and B. Wang, *J. Raman Spectrosc.*, 2012, **43**, 863–868.
20 S. M. Morton, D. W. Silverstien and L. Jensen, *Chem. Rev.*, 2011, **111**, 3962–3994.
21 S. Schlücker, *Surface Enhanced Raman Spectroscopy*, Wiley-VCH Verlag & Co., Weinheim, Germany, 2011.
22 J. Crank, *The Mathematics of Diffusion*, Oxford, Oxford, England, 2nd edn, 2011.
23 The Flory–Huggins interaction parameter for this polymer pair is weakly unfavorable (positive), as reported in P. F. Green and B. L. Doyle, *Macromolecules*, 1987, **20**, 10–12. For the molecular weights employed in this work (200 000 g mol^{-1}), the Flory–Huggins model predicts an upper critical temperature of 150 K. Thus, at any temperature above that value, the system is in the one-phase region of the phase diagram.
24 E. J. Kramer, P. Green and C. J. Palmstrom, *Polymer*, 1984, **25**, 473–480.
25 F. Brochard, J. Jouffroy and P. Levinson, *Macromolecules*, 1983, **16**, 1638–1641.
26 R. J. Composto, E. J. Kramer and D. M. White, *Macromolecules*, 1988, **21**, 2580–2588.
27 P. F. Green and E. J. Kramer, *Macromolecules*, 1986, **19**, 1108–1114.